Journal of Sciences, Islamic Republic of Iran 24(3): 217-228 (2013) http://jsciences.ut.ac.ir
University of Tehran, ISSN 1016-1104

Oligocene partial melting in the Takab metamorphic complex, NW Iran: Evidence from in situ U-Pb geochronology

M. Moazzen[1,*] , R. Hajialioghli[1], A. Möller[2], G.T.R. Droop[3], R. Oberhänsli[4], U. Altenberger[4], A. Jahangiri[1]

[1] *Department of Geology,Faculty of Natural Sciences, University of Tabriz, 51664 Tabriz, Islamic Republic of Iran*

[2] *Department of Geology, University of Kansas, Lawrence, Kansas, USA*

[3] *School of Earth, Atmospheric and Environmental Sciences, University of Manchester, UK*

[4]*Institut für Erd- und Umweltwissenschaften, Universität Potsdam, Potsdam, Germany*

Received: 1 June 2013 / Revised: 18 July 2013 / Accepted: 6 August 2013

Abstract

U-Pb ages obtained on zircons from the investigated migmatites place new constraints on the evolution of the crustal rocks in the Takab area. SHRIMP U-Pb dating of inherited zircon in the melanosome parts of mafic migmatites from the Takab complex gives a discordant age with an upper intercept of 2961±72 Ma (MSWD=0.5) and a lower intercept of 24.2±5.7 Ma (MSWD=1.7). In the concordia diagram, the melt-grown zircons yield a more precise age of 25.67±0.74 Ma (MSWD=1.7), similar to the lower intercept age of the discordia. At least part of the scatter along the concordia for the new zircon generations may be real, caused by an extended period of melting and crystallization, in which case the oldest age of c. 29 Ma dates the onset of partial melting. The Oligocene ages for the younger zircons show the importance of partial melting in these mafic rocks. The typical euhedral to subhedral shapes are features related to crystallization and resorption of the grains due to *in situ* melting. These processes were most likely related to the generation of the Tertiary granitoids of the Takab complex.

Keywords: SHRIMP dating; mafic migmatites; Takab

Introduction

The Takab metamorphic complex of northwestern Iran is located between longitude 37º30′-36º30′N and latitude 47º45′-47º5′E and is one of several outcrops of pre-Tertiary crystalline basement in Iran. In the context of the structural subdivisions of Iran, the complex has been assigned to various tectonic zones by different

* Corresponding author, Tel.: 0098-411-3392679, Fax: 0098-411-3356027, E-mail: Moazzen@tabrizu.ac.ir

workers. It is considered to be part of the Central Iran Zone by [32], the Sanandaj-Sirjan Zone [8] and at the junction of the Central Iran, Sanandaj-Sirjan and Alborz-Azerbaijan zones (Fig. 1).

Traditionally, the Takab Complex has been viewed as a continental fragment with Gondwanan affinity, despite the fact that evidence from isotopic dating has largely been lacking. Lithologically, the complex consists of a variety of rocks including granulites, amphibolites, calc-silicates, meta-ultramafites, orthogneisses and pelitic schists [10, 11, 27] (Fig. 1). The rocks record polyphase deformation, magmatism and Barrovian-type metamorphism, most likely related to both Pan-African and Alpine orogenies. Mafic migmatites, which formed during high-grade metamorphism, may be related to subduction and subsequent collision following the closure of Neotethys in the Tertiary. Outcrops of crustally derived granitoids commonly occur in close association with the migmatites in the area [12].

Unravelling the geological history of NW Iran has been hampered by lack of firm geochronological data. The age of the oldest components of the Iranian crystalline basement is a key issue for establishing the extent to which the Pan-African orogeny involved reworking of older Precambrian continental crust or, alternatively, the addition of juvenile crust. The age of partial melting in the migmatites is also crucial as it will confirm or refute a connection with Neotethyan subduction and Tertiary granitoids in the area. In this paper, we use U-Pb zircon geochronology to address these two issues.

This investigation focuses on *in situ* U-Pb isotopic dating of zircon from metabasic migmatites in the Takab metamorphic complex. We present evidence that the Takab migmatites contain two populations of zircon: (i) relict zircons of Archaean age, and (ii) melt-grown zircons of Tertiary age. The implication of these findings for the geodynamic evolution of the region will be addressed.

Zircon, essentially $ZrSiO_4$, is a common accessory mineral in crustal rocks and has a number of attributes that render its usefulness for U-Pb geochronology: (i) U can substitute for Zr in its crystal lattice; (ii) Pb, the ultimate stable daughter element produced by radioactive decay of U, diffuses through its lattice with great difficulty, with the result that crystals close to Pb diffusion at temperatures in excess of 900°C [28]. Most studies of zircon in metamorphic rocks have utilized mineral separates, but this has the disadvantage that key textural relationships between zircon and its surrounding minerals are lost, leading to loss of

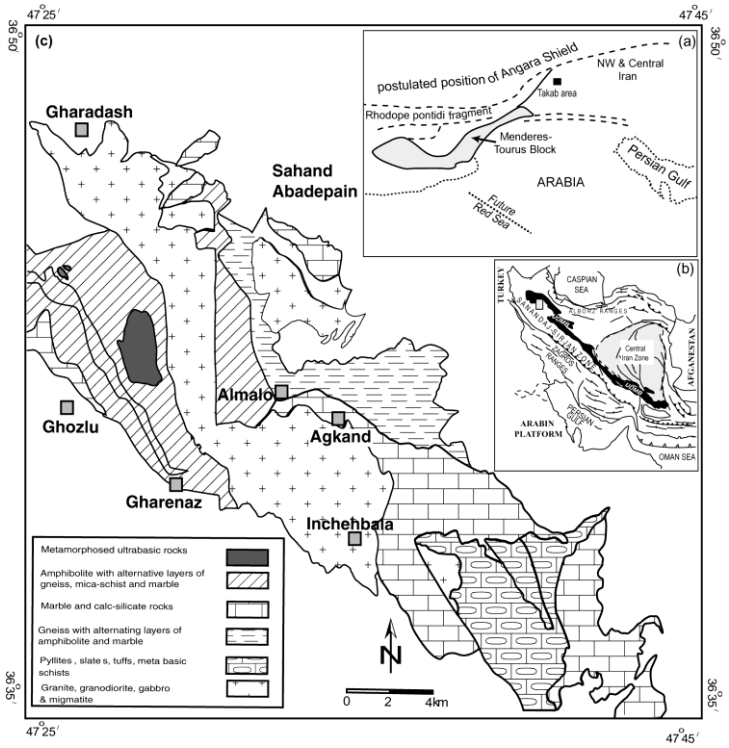

Figure 1. (a) Palaeozoic reconstruction of terranes in Turkey and Iran (after [40]); (b) Structural subdivision of Iran (after [8]). (c) Geological map of the study area, adapted from the geological map of Takht-e-Solyman [22] with some modifications.

information on the role of zircon in local metamorphic processes. However, recent instrumental developments have enabled *in situ* dating of zircon at high spatial resolution directly on thin sections, with the great advantage of preserving textural information [18, 20, 29, 35], and we use this technique in this study.

Regional overview of the Iranian crystalline basements and the adjacent areas

The ages of the oldest rocks of the Iranian crust have been poorly constrained and are controversial. Previous Rb-Sr geochronological work has assigned Precambrian [36] and Archaean ages to the Iranian crystalline basement. Samani et al. [39] reported Mid-Proterozoic U-Pb isotopic ages for granitoids in the Central Iran Zone. Ramezani and Tucker [36] and Verdel et al. [44] reported Neoproterozoic-Cambrian U-Pb zircon ages of 543±36 Ma for the oldest rocks of the Iranian crust from metmaorphic rocks of the Saghand area in the Central Iran Zone, with some older inherited components. Nadimi [33] documented a U-Pb zircon age of 2400 Ma for the oldest basement complexes of the Central Iran Zone, corresponding to the Palaeoproterozoic 'Chapedonian' Orogeny. Based on these results and similarities in lithology and stratigraphy, a Proterozoic age was also proposed for the protoliths of the Takab complex [10, 11]. Recently, Hassanzadeh et al. [13] documented Neoproterozoic to Early Cambrian granitoids and granitic gneisses in the crustal basement assemblage of the Iranian terrane (i.e. Zagros, Sanandaj-Sirjan, Alborz and Central Iran zones), with some indications for Proterozoic (ca. 1070 Ma and ca. 1450 Ma) inherited or detrital zircon in the youngest granitiod, of Pleistocene age. Crust of similar Neoproterozoic crystallization ages has been documented from the Arabian platform [42], the Bitlis Zone of south eastern Turkey [34] and the Menderes Massif core complex in western Turkey [14]. Neoproterozoic palaeogeographic reconstructions place the Iranian terrane along the Prototethys margin of Gondwana between the Zagros margin of Arabia and the NW margin of the India plate. Consolidation of the basement rocks throughout the Iranian plate is thought to have occurred during the Neoproterozoic-Early Cambrian Pan-African Orogeny [42]. The basement rocks in the Iranian plate, which consist of orthogneisses, metabasites and metasediments, have been correlated with the Pan-African metamorphic terranes of the Arabian-Nubian Shield and Turkey by Nadimi [33]. Following the Pan-African Orogeny, crustal extension resulted in (i) the opening of Neotethys and the concomitant translocation of the Gondwanan blocks of Iran from the Arabian-Nubian shield to the Eurasian shield as Palaeotethys closed [13], and (ii) the related magmatism. The protoliths of the orthogneisses from the Takab core complex correlate with the post-orogenic magmatic activity of the Pan-African Orogeny [13] analogous to similar compositions from the Central Iran Zone, Arabia and Turkey (see section on Pre-Pan African crust in the Takab and adjacent areas below).

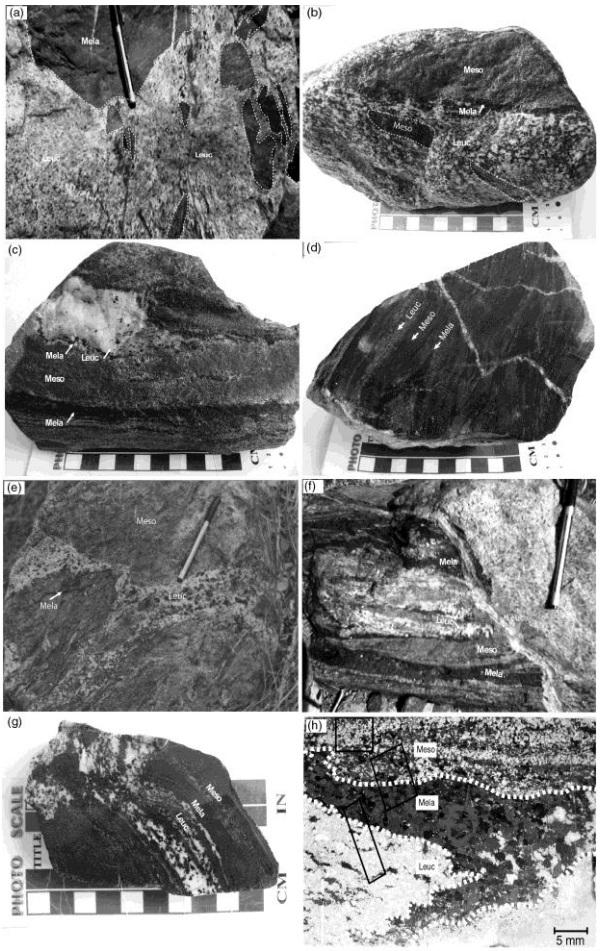

Figure 2. Mesoscopic structure of the mafic migmatites from the Takab area. (a) Schlieren migmatite includes floating elongated melanocratic fragments. (b) A thin hornblende-rich melanosome is developed around mesosome. Metabasic rafts or schollen occur in the leucosome. (c) Melanosome selvage around leucosome. (d) Nebulite structure is seen as homogeneous distribution of leucosome. (e) Coarse grained pegmatitic diatexite composed of plagioclase and amphibole megacrysts (f, g) Stromatic migmatites showing concordant migmatitic elements including leucosome, mesosome and melanosome in the layered migmatites. (h) Photomicrograph of the diatexite migmatite sample R-29a having millimetre-scale distinct migmatitic elements selected for zircon U-Pb isotopic dating.

Geological setting

The Takab metamorphic core complex outcrops with a general NW–SE trend parallel to the Zagros suture zone, within the Alpine-Himalayan orogenic belt. The metamorphic complex has been thrust over the Miocene volcanosedimentary rocks along the NW–SE Qeynarj-e-Chartagh thrust fault (Fig. 1). The earliest significant basement exhumation occurred during Early to Middle Jurassic back-arc extension [13]. Large-scale crustal extension and exhumation related to the Tertiary collisional tectonics probably also helped to expose the basement rocks in the study area (e.g. [13]). Polyphase metamorphism and deformation related to the Pan-African, Triassic (?) and Alpine orogenies affected the rocks in the Takab area. The nature and extent of the pre-Pan-African processes are debated and require further study.

Lithologically, the Takab metamorphic complex is composed of garnetiferous pelitic and psammitic gneisses, intercalated with pelitic and psammitic schists, marbles and garnet amphibolites of presumable volcanic origin (Fig. 1). Granulites are exposed sporadically in the area. Meta-ultramafic rocks crop out as thin, elongated layers and discontinuous small bodies commonly within amphibolite. Amphibolites occur mainly in the northern part of the complex whereas gneisses dominate in the south (Fig. 1). The mafic migmatites formed by partial melting of the metabasites, a process which is thought to have been related to continental collision during the Alpine Orogeny. Granitoids occur sporadically in the area in association with the mafic migmatites [12]. The crucial evidence for the relative age of the granitoids and associated mafic migmatites is provided by the field relationships (see below). Tertiary volcanic and sedimentary rocks and recent alluvial deposits overlie the metamorphic rocks uncomformably.

The Takab mafic migmatites

Mafic migmatites in the Takab metamorphic complex outcrop near the Gharenaz village (Fig. 1). Migmatite terminology used in this study follows the definitions of Mehnert [25]. The terms ‘leucosome’, ‘mesosome’ and ‘melanosome’ are used to describe migmatite components with light (quartzo-feldspathic), medium and dark colours, respectively.

The Takab migmatites are structurally heterogeneous. Leucosomes occur on scales of several millimetres to tens of centimetres either as leucosome layers in stromatic and schlieren migmatites or as discrete veins. Mineral assemblages include coarse-grained plagioclase and hornblende together with minor K-feldspar and quartz. They have granodioritic-tonalitic compositions with typical granular texture. Hornblende-rich layers ranging from 1mm to a few cm in thickness typify the melanosomes and occupy more than 50% by volume on average at the outcrop scale. They are composed dominantly of hornblende (40-90 vol.%), plagioclase and opaque phases. Hornblende crystals in melanosomes reach 2.5 mm in length and are coarser than in mesosomes. Mesosomes consist of medium- to fine-grained, foliated amphibolite with less than ~35 volume % hornblende (estimated at the outcrop scale). The mineral assemblage of the mesosomes is the same as that of the melanosomes, but with a smaller hornblende proportion. The dominant assemblage of the mesosomes is plagioclase and hornblende. Quartz and K-feldspar occur in minor amounts.

Schlieren migmatites of the area are defined by disaggregated ‘floating’ melanocratic fragments which are aligned parallel to the melt flow (Fig. 2a). In some samples, melanosomes occur as thin selvages around mesosomes (Fig. 2b) and/or leucosomes (Fig. 2c). A relatively homogeneous distribution of leucosome forms a nebulitic structure in some samples (Fig. 2d). Locally the leucosomes contain semi-digested metabasic rafts or schollen from which the melt is largely derived (Fig. 2b). The size and shape of fragments are dependent on protolith composition. Infrequently, coarse-grained pegmatoid veins, composed of plagioclase and amphibole megacrysts, occupy fractures (Fig. 2e). In stromatic migmatites, compositional layering is marked by alternating cm-scale light-coloured quartzo-feldspathic layers (leucosomes) and dark hornblende-rich layers (melanosomes) (Fig. 2f). This may be interpreted as the result of extensive partial melting and accumulation of melt along certain layers, thus enhancing the layered structure. Fig. 2g shows concordant leucosome, mesosome and melanosome in a stromatic migmatite. Mesosomes are absent from some metabasic migmatites.

A migmatite with distinct millimetre-scale leucosome, melanosome and mesosome (sample R-29a) was selected for zircon U-Pb isotopic dating (Fig. 2h).

Zircon description

Zircon types were identified by petrography, morphology, grain size and modal abundances within the leucosomes, melanosomes and mesosomes of the migmatites. The zircon grains were also examined carefully by back-scattered-electron (BSE) and cathodoluminescence (CL) imaging and ion microprobe analysis (U-Pb zircon analysis by SHRIMPII). Zircons

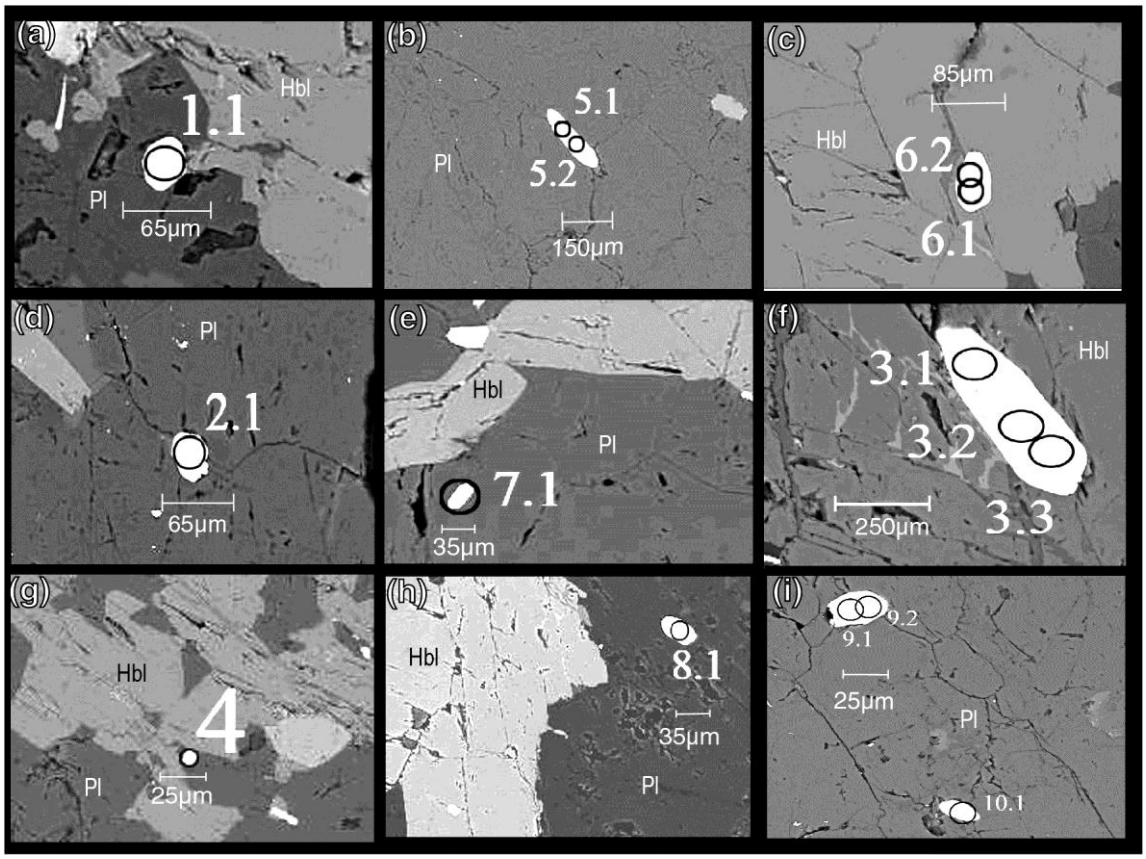

Figure 3. Backscattered electron (BSE) images of zircon in the investigated migmatites. Circles show the position of SHRIMP analysis: (a) inherited zircon in the melanosome; (b-d) melt grown zircons in the mesosome; (e-g) the leucosome; and (h-i) the melanosome. The BSE images demonstrate that the leucosome and the melanosome have coarser and more abundant zircon grains than the mesosome. Pl (plagioclase) and Hbl (hornblende).

in the different portions of the migmatites differ in grain size, distribution and morphology. In general, the Takab mafic migmatites contain very low modal proportions of zircon, which can be explained either by the scarcity of this mineral in the mafic igneous protoliths or by the growth during metamorphism of Zr-bearing phases such as hornblende, biotite and ilmenite progressively absorbing Zr and inhibiting zircon growth (e.g. [49]).

In the mesosome of sample R-29a, zircon is scarce, generally occurring as rare subhedral to rounded grains ranging in length from 35 to 50µm (Fig. 3a).

Zircons in the leucosome and melanosome of sample R-29a are more abundant and larger than those in the mesosome. They are typically subhedral to anhedral prisms with aspect ratios of 1:2 to 1:3, ranging in length from 50 to 500µm (Fig. 3e-i). Rare crystals of this type also occur in the mesosome (Fig. 3b-d). These zircons appear to have crystallized as simple, new grains, and their oscillatory and sector zoning are typical grain growth from melt. We therefore interpret these zircons as melt-grown crystals. In the melanosome, some of the zircon prisms contain distinct rounded cores overgrown by new zircon. Core-rim boundaries are sharp. The cores show weak luminescence which may be modified by metamorphic recrystallization. We interpret the cores as relics of zircon crystals that were present in the metabasites prior to migmatization.

The relatively high modal amounts of zircon in the melanosome and the leucosome can be interpreted as the result of elevated Zr released by resorption of Zr-bearing silicates in metamorphic reactions or by dissolution of older zircon grains during partial melting and subsequent crystallization from this melt.

Zircon U-Pb dating

Chips of the leucosome, mesosome and melanosome of the selected migmatite sample R-29a were mounted in epoxy resin. Geostandard reference zircons (91500) were located in a different SHRIMP-mount. All measurements were carried out *in situ* on polished thin sections. Backscattered electron (BSE) images were

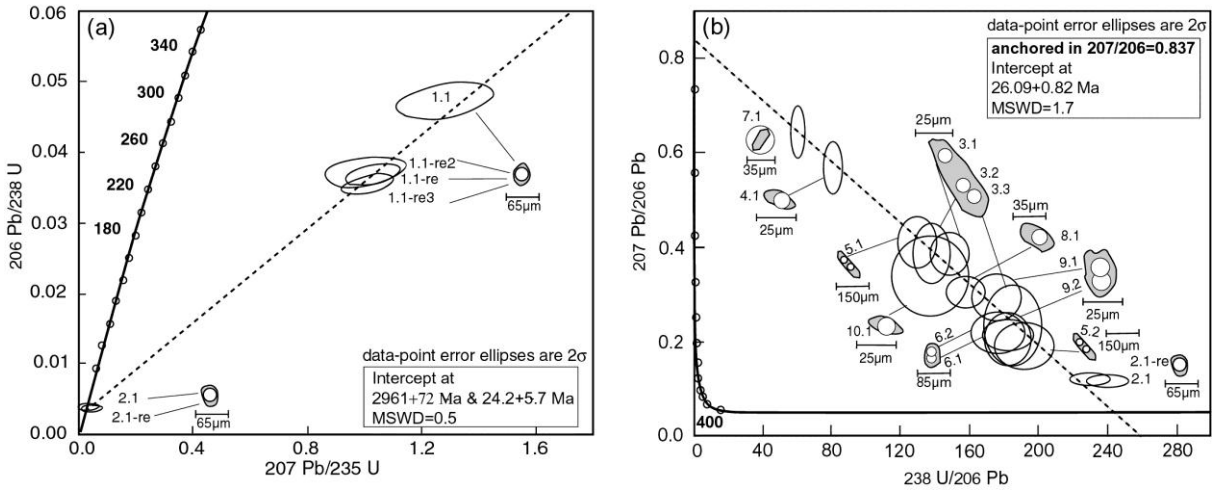

Figure 4. (a) Zircon U-Pb concordia diagram for migmatites from the Takab complex. (a) Wetherill type; and (b) Tera-Wasserburg type. The inherited zircons yield isochron intercept ages of 2961±72 Ma and 24.2±5.7 with MSWD=0.5 in Wetherill concordia space. The U-Pb ages for other zircon grains are consistent at c. 26 Ma in the Tera-Wasserburg diagrams. Ellipses represent 2σ errors. $^{206}Pb/^{238}U$ ages (Ma) are given for each spot analysis with 2σ error $^{206}Pb/^{238}U$ ages in bracket are from discordant U-Pb data.

taken as a guide for selection of spots for U-Pb dating analysis. Fig. 3 shows BSE images with marked analysis points. U-Pb isotopic measurements were performed using the sensitive high-resolution ion microprobe (SHRIMP II) at the Centre of Isotopic Research (CIR) All-Russian Geological Research Institute (VSEGEI), Saint Petersburg (Russia). The primary beam intensity was about 2.5 nA and the sputtered secondary ions were accelerated with a voltage of 10 kV. Each analysis consisted of five scans through the mass range, and the diameter of the measurement spot was 20-25µm. Because of the small grain sizes, only a single spot analysis on each zircon was possible for U-Pb dating on most grains. A total of 19 *in situ* SHRIMP analyses were obtained, 6 analyses from rounded cores in the melanosome, 6 analyses from zircons in mesosome and 7 analyses from zircons in leucosome (Table 1).

The data were reduced in a manner similar to that described by Williams ([47], and references therein), using the SQUID Excel Macro program of [23]. The Pb/U ratios were normalized relative to a value of 0.17917 for the $^{206}Pb/^{238}U$ ratio of the 91500 reference zircons, equivalent to an age of 1062.4 Ma [46]. Uncertainties given for individual analysis (ratios and ages) are at the 1σ level; however, the uncertainties in calculated concordia ages are reported at the 2σ level. Ahrens-Wetherill [1, 45] and the Tera-Wasserburg [43] concordia plots were prepared using ISOPLOT/EX [25]. It is generally accepted that the Tera-Wasserburg type of concordia diagram allows to better calculate and visualize the intersection between the concordia curve and discordia lines for young ages (<1.0 Ga) than the Wetherill diagram.

U-Pb geochronological results

The data yield two groups of ages. Four spot analyses on rounded zircon cores from the melanosome yield discordant $^{206}Pb/^{238}U$ ages of 223-299 Ma (Table 1). They define a discordia chord with two intercept ages of 2961±72 Ma and 24.2±5.7 Ma, respectively in the Wetherill concordia space (MSWD=0.5; Fig. 4a). The low MSWD is a result of the large errors on the older four, discordant analyses, which also dominate the slope and error on the lower intercept. The age and error of the lower intercept should therefore be just used as an approximation. Detailed interpretation of the younger cluster of data is best done with a Tera-Wasserburg concordia diagram that excludes the older analyses. The upper intercept, points to the inheritance of Archaean material in the analysed grain, which was verified by several repeat analyses. The discordant nature of these analyses is attributed to overlap of the analyses spot on Archaean inherited and migmatitic overgrowth zircon material.

All the other 15 analysed spots have relatively high common lead contents, so the $^{206}Pb/^{238}U$ ages with correction based on ^{207}Pb reveal the least scatter, ranging between 24.5-29.6 Ma, whereas ^{204}Pb corrected data show very large scatter (see Table 1). The Tera-

Wasserburg concordia diagrams show the data without correction for common lead (Fig. 4b).

The U-Pb data (excepting low-common-Pb zircons) were plotted in a manner described by [3]. Assuming concordance of ages, the mixing line between common and radiogenic lead was plotted. The lower intercept of this line with concordia gives the age of the zircons. The radiogenic Pb content was low, but the Tera-Wasserburg concordia diagram plotted for the uncorrected data yields a well-defined regression line with an age of 25.67±0.74 Ma (MSWD=1.7). This age is indistinguishable within error from the age of 26.09±0.82 Ma (MSWD=1.7) defined by a regression line forced through the point reflecting the Pb composition in the SHRIMP-II laboratory at CIR (Fig. 4 b). Note that the most U-rich zircon (grain 2) is the least discordant and lies slightly off the discordia line (Fig. 4 b). This is weak evidence showing that this grain is slightly younger than the rest, producing the excess scatter.

The ages acquired in the Tera-Wasserburg concordia diagram are consistent with the relatively imprecise lower intercept age of the Wetherill concordia (Fig. 4 a).

The scatter in the U-Pb isotopic data along the concordia may be caused by varying amounts of common Pb present in the zircon related to Pb/U differentiation during zircon growth [50, 51]. Alternatively, the scatter is real and reflects crystallization of melt and zircon over an extended period of time, longer than the 0.82 Ma, as advocated by [37] for partial melts in high grade rock units of the European Alps.

Th and U contents in zircon

The isotopic data presented here suggest that there is systematic difference in age related to the U content (Fig. 5a). Due to long ingrowths of radiogenic Pb, the old grains have high radiogenic ^{206}Pb and low common lead ^{204}Pb, whereas the grains with young ages mostly are characterized by high ^{204}Pb and low radiogenic Pb (Table 1). The high U concentrations in one of the young zircon grains (spot 2.1 and 2.1-re; Table 1) can be interpreted as being related to breakdown of a U-bearing mineral in the melt source rock (providing a higher U melt). This high-U zircon grain has among the youngest ages in the U vs. ^{206}Pb/^{238}U age diagram (Fig. 5a). There is also a positive correlation between U (ppm) and Th (ppm) which may be related to fractionation of the source melt where zircon growth depletes the melt effectively in Th, U and HREE (Fig. 5b) (e.g. [29]). The Th/U plot shows that the young high U grain (grain 2) does not follow the general Th/U trend.

It has been suggested by some authors that the Th/U ratios of zircons can help to discriminate between

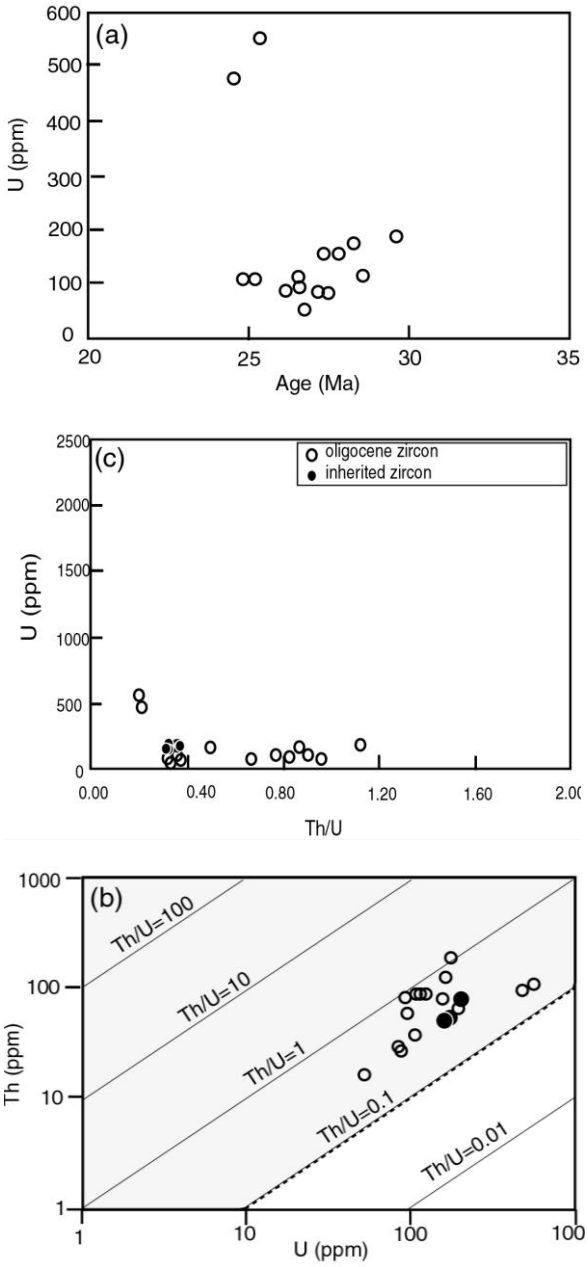

Figure 5. (a) U concentration (ppm) vs. ^{206}Pb/^{238}U age diagram for the Oligocene zircon grains in the investigated migmatites. The high U concentrations in one of the young zircon grains (spot 2.1 and 2.1-re) can be interpreted as being related to breakdown of a U-bearing mineral in the melt source rock. (b) U (ppm) vs. Th/U (ppm) diagram suggests fractionation of the source melt. (c) Th/U vs. U (ppm) difference between newly crystallized zircons and inherited zircons.

magmatic and metamorphic growth [48]. It is interesting that the new zircons of the investigated rocks span a very wide range of Th/U ratio, from 0.20 to 1.10, irrespective of position in leuco-, meso-, and melanosome (Fig. 5c). Moderate to high Th/U ratios are typical of melt-grown zircons (Fig. 5c) (e.g. [29, 30, 48]). The mechanism by which the Th/U ratio is enhanced in magmatic processes and reduced in metamorphism is poorly understood. High ratios may reflect Th-U partitioning and fractionation between melt and zircon coupled with the high Th/U nature of the high-temperature melt. Möller at al. [29] suggest that Th/U is variable between zircon populations and that higher Th/U values occur within larger zircon grains and vice versa. This is clearly not the case for the investigated rocks because the Th/U ratio does not correlate with the size of zircon grains in our rocks (see Fig. 4b).

Results and Discussion

In this study we investigated zircons in the mesosome, leucosome and melanosome of a mafic migmatite to provide the connection between zircon growth and partial melting. On the basis of zircon morphology we deduce that the Takab basic migmatites contain two types of zircon: inherited and melt-grown.

Inherited zircon grains

Zircon grains are often inherited or contain inherited parts, which has been defined by [17] to be caused by entrainment in melts in igneous rocks, whereas it may be caused by preservation of previously existing zircon during metamorphism (including partial melting) or from detrital sources. Preservation or inheritance of pre-existing zircon is then determined by kinetics and the rate of igneous and metamorphic processes (e.g. sluggish kinetics of reactions or fast, short-lived magmatic and metamorphic processes; [17]). The preservation of pre-existing zircon in metamorphic rocks also requires that the temperature at which 100% dissolution occurs was not exceeded along the P-T path.

Inherited zircon in the Takab migmatites occurs occasionally as rounded cores to some of the zircon prisms that are inclusions in hornblende and plagioclase in the melanosome, while it is likely that most of the inherited zircons were lost via dissolution during prograde metamorphism.

Formation of zircon during partial melting

The majority of zircons in the investigated migmatitic samples crystallized during partial melting. They occur either as zoned rims on pre-existing grains or as newly grown crystals. They are commonly subhedral to rounded, and only rarely preserve perfect euhedral shapes. This type of zircon is well documented and is generally interpreted as zircon that has grown in the presence of melt during partial melting (e.g. [16, 37].

The rounded edges of these prismatic zircon grains point to resorption by melt (Fig. 3e-f). Resorption and unzoned structures in zircon are documented as distinct textural relations that suggest zircon formed by *in situ* recrystallization rather than by precipitation from a melt. Oscillatory and sector zoning in the studied zircons point to their generation from a discrete melt, i.e. anatectic melt. Their constant modal proportions in the melanosomes and the leucosomes also suggest formation as a result of *in situ* melting.

Three mechanisms for zircon growth during partial melting can be considered: (i) dissolution-reprecipitation of pre-existing zircon [16], (ii) breakdown of Zr-bearing phases other than zircon in a closed system [7]; (iii) crystallization from externally derived Zr-bearing melt.

On the basis of textural relations and mineralogical evidence, it is conceivable that growth of new zircon in the investigated migmatites may be linked to breakdown of Zr-bearing phases such as amphibole, pyroxene, garnet and ilmenite, all of which may contain tens of ppm Zr [7]. However, it is also possible that the Zr required for zircon growth was contributed by partial or complete dissolution of pre-existing zircon grains (e.g. [38]), a mechanism that could also help to explain the attrition of the rounded cores.

The relatively large size of the melt-grown zircons may be interpreted to relate to zircon undersaturation conditions during partial melting. The new zircons are internally homogeneous, and therefore do not suggest multiple stages of zircon growth within grains.

Significance of U-Pb ages

The presented U-Pb isotopic data suggest that the Takab migmatites contain two types of zircon. As the analysis was carried out *in situ*, the precise petrographic setting of each analyzed zircon is known. Thus we can interpret that the young zircons are newly grown grains crystallized in relationship with partial melting and partial melt crystallization and the old zircons as inherited. The presence of only one, Archaean, distinct inherited component allow us to interpret the significance of the dates obtained with respect to the migmatization event. U-Pb data from the migmatites

Table 1. SHRIMP zircon U-Pb isotopic data for the leucosome, melanosome and mesosome of mafic migmatites in the Takab metamorphic complex. Mela (melanosome), Leuco (leucosome) and Meso (mesosome).

^{208}Pb cor $^{206}Pb/^{238}U$ Age	1σ err	^{207}Pb cor $^{206}Pb/^{238}U$ Age	1σ err	^{204}Pb cor $^{207}Pb/^{206}Pb$ Age	1σ err	^{204}Pb cor $^{206}Pb/^{238}U$ Age	err cor	% err	$^{206}Pb/^{238}U$	% err	$^{207}Pb/^{235}U$	% err	$^{207}Pb/^{206}Pb$	% err	$^{238}U/^{206}Pb$	% err	Total $^{207}Pb/^{206}Pb$	% err	Total $^{238}U/^{206}Pb$	ppm rad ^{206}Pb	$^{232}Th/^{238}U$	ppm Th	ppm U	%com ^{206}Pb	Spot name	Textural type of zircon
317.7	4.6	244.2	83	2795	6.3	298.3	.39	2.1	.047	5.5	1.28	5.0	.196	2.1	21.11	1.7	.240	1.6	19.65	8.6	0.37	72	198	6.91	1.1 (mela)	Small and subhedral
250.6	3.8	193.8	92	2775	5.3	236.4	.38	2.3	.037	6.1	1.00	5.6	.194	2.3	26.78	2.0	.230	1.7	25.25	6.1	0.33	58	179	5.70	1.1-re (mela)	Small and subhedral
25.4	0.6	25.4	1050	544	1.0	25.7	.08	4.1	.004	48.2	0.03	48.0	.058	4.1	249.96	4.7	.122	2.1	229.49	2.1	0.20	106	551	8.19	2.1 (meso)	Small and rounded
24.6	0.5	24.5	1419	-37	1.0	24.5	.07	3.9	.004	58.6	0.02	58.4	.045	3.9	262.93	4.4	.116	2.1	239.44	1.7	0.21	97	482	8.93	2.1-re (meso)	Small and rounded
26.8	1.3	24.8	1326	2318	4.6	28.4	.21	16.4	.004	79.0	0.09	77.3	.148	16.4	226.31	4.8	.386	3.2	148.0	0.6	0.36	38	107	34.6	3.1 (leuc)	Large and anhedral
25.5	1.8	26.6	375	3227	3.4	36.2	.37	9.3	.006	25.5	0.20	23.7	.257	9.3	177.51	6.8	.387	3.3	137.7	0.7	0.83	89	111	22.43	3.2 (leuc)	Large and anhedral
26.8	1.8	26.6			3.5	25.3		13.9	.004					13.9	253.83	15	.234	3.8	184.64	0.4	0.66	60	94	27.26	3.3 (leuc)	Large and anhedral
25.4	2.6	27.2	417	3760	8.8	45.2	.579	19.5	.007	33.7	0.35	27.5	.362	19.5	142.05	3.9	.568	3.0	80.40	1.0	0.32	27	89	43.4	4.1 (mela)	Small and subhedral
29.5	1.7	26.7			9.6	16.7		57.6	.003					57.6	384.57	5.4	.411	3.5	129.4	0.4	0.33	17	53	66.35	5.1 (meso)	Large and euhedral
27.2	1.3	27.4	1091	1610	2.4	29.4	.14	8.1	.005	59.1	0.06	58.6	.099	8.1	219.10	11	.192	3.7	191.54	0.4	0.37	30	85	12.58	5.2 (meso)	Large and euhedral
27.7	1.1	27.7	3455	325	3.0	28.0		10.6	.004					10.6	230.07	6.3	.217	3.4	181.94	0.7	0.87	132	157	20.92	6.1 (meso)	Medium & anhedral
28.5	1.4	28.5	369	2460	1.9	33.3	.253	5.7	.005	22.5	0.11	21.8	.160	5.7	193.23	8.1	.220	3.7	176.31	0.6	0.77	88	119	8.76	6.2 (meso)	Medium & anhedral
32.1	3.5	26.2	1291	3340	14.3	36.8	.43	39.0	.006	91.3	0.22	82.6	.28	39.0	174.51	3.5	.644	2.8	59.90	1.3	0.96	83	90	65.67	7.1 (mela)	Small and euhedral
28.8	1.1	27.4	1230	1986	3.6	30.3	.17	11.9	.005	70.1	0.08	69.1	.12	11.9	212.36	4.5	.305	2.8	158.01	0.9	0.50	76	157	25.59	8.1 (leuc)	Small and anhedral
26.5	1.3	25.2	297	2990	2.1	32.3	.33	6.4	.005	19.6	0.15	18.5	.221	6.4	198.95	7.0	.293	3.4	175.59	0.5	0.90	94	108	11.74	9.1 (leuc)	Small and anhedral
30.6	2.9	29.6	1970	1864	5.5	32.3		17.1	.005					17.1	198.85	10	.339	6.7	136.93	1.2	0.36	65	188	31.14	10.1 (leuc)	Small and anhedral
28.8	1.3	28.3	2650	599	2.6	28.8		9.2	.005					9.2	223.70	11	.205	2.9	181.86	0.8	1.12	189	175	18.7	9.2 (leuc)	Small and subhedral
242.7	3.5	189.2	55	2842	4.3	233.7	.48	1.9	.037	3.9	1.03	3.4	.202	1.9	27.08	1.9	.215	1.6	26.52	5.3	0.32	50	164	2.07	1.1-re2 (mela)	Small and subhedral
233.4	3.4	180.6	53	2875	4.1	224.7	.50	1.9	.036	3.7	1.01	3.2	.206	1.9	28.20	2.0	.219	1.7	27.62	5.0	0.33	51	162	2.05	1.1-re3 (mela)	Small and subhedral

indicate partial melting at 26.09±0.82 Ma (MSWD=1.7), with the possible latest pulse of high-U zircon crystallization at 24.9 ±0.8 Ma (weighted average of grain2 analyses). These ages are interpreted as most likely corresponding to the growth of zircon during Oligocene partial melting.

The inherited zircon has a U-Pb upper intercept age of 2961±72 Ma (within uncertainties) and may indicate crystallization of zircon in the igneous protolith, therefore providing a minimum age of crust formation.

The c. 2961 Ma age obtained by SHRIMP analysis on inherited zircon in the melanosome is interpreted as the possible age of relict zircon grains in the Takab crustal basement. Other pre-Tertiary zircon populations were not found in the mesosome of the investigated migmatite. This does not prove the absence of other metamorphic episodes in the area as it could merely be a symptom of unavailability of fluid or melt during metamorphism. Zircon crystallization during metamorphism is apparently an extremely sluggish process in the absence of fluid to catalyze growth or recrystallization. Another possibility is that the high degree of partial melting in the area resulted in resorption of earlier metamorphic zircon grains in mesosomes of the investigated rocks. High grade metamorphism in the area is documented by [27].

The age of the mafic migmatites and their significance in the geological evolution of the Takab area have been obscure up to now. Based on field geological relationships, geological observations and geochronological data, the age of migmatization has long been assumed to be Tertiary by previous research groups. Our data demonstrate that this assumption is correct. SHRIMP zircon U-Pb dating of the different subhedral to euhedral new zircon crystals constrains the timing of partial melting. The spread of ages may be interpreted as recording the presence of melt through the time interval of c. 29 to 25 Ma (also see [37] for comparison). The isotopic data suggest that zircon growth began at c. 29 Ma and possibly continued until c. 25 Ma. This range of zircon growth ages implies a duration for the partial melting of up to 4 Ma, whereas the mean age is defined to 26.09±0.82 Ma with a MSWD=1.7 that indicates excess scatter. The morphology and textural features of the analysed zircons all support an origin by precipitation from melt.

Pre-Pan African crust in the Takab and the adjacent areas

The Takab metamorphic core complex has many similarities with the crystalline rocks of the Central Iran Zone [10] and is located in the western continuation of the Menderes-Taurus Block (Fig. 1a). The crystalline basement of the Bitlis Massif and the Zagros Zone of western Iran have been documented as a coherent block

forming the northern continuation of the Arabian platform as they record a similar palaeogeographic evolution from Precambrian to Early Cambrian times involving sequential opening and closing of Palaeotethys and Neotethys oceans [9]. Also, the intrusion ages of the granitic gneisses in the Takab metamorphic complex (~560 Ma; U/Pb zircon, [41]) are similar to U-Pb dates from basement rocks of the Saghand area in the Central Iran Zone (c. 540 Ma, [36]) and the Menderes Massif (c. 550 Ma; [5]).

Late Archaean to Palaeoproterozoic magmatic activity in Turkey is recorded by orthogneisses with $^{207}Pb/^{206}Pb$ zircon ages ranging from 2,555 to 1,740 Ma [21], but up to now no evidence for pre-Pan-African activity has been obtained from the crystalline basement rocks of the Takab complex (or, indeed, from anywhere in the Iranian crust). Our U-Pb ages with upper intercepts of c. 2900 Ma indicating Archaean migmatite protoliths might correspond to a phase of Archaean magmatic activity in the study area. More importantly, our results also suggest that the crystalline basement of Iran is not entirely composed of juvenile Pan-African crust, but contains some inherited older components, as do the eastern Arabian shield and Menderes Massif, and that like these massifs, at least part of the Iranian crust is a continental fragment with Pre-Gondwanan affinity.

Tectonic implications

There is an unconformity between the metamorphosed Neoproterozoic–Early Cambrian rocks and the overlying Cambrian rocks in the Takab area. Thick dolomitic marbles are interlayered with volcaniclastic and volcanic rocks, corresponding to deepwater, turbiditic environments. The ultramafic rocks of the Takab area are considered to be remnants of the Proto-Tethyan oceanic lithosphere which was obducted during Pan-African continental collision [10]. A similar tectonic scenario has been documented for the Central Iran Zone by [36].

The inherited zircons of the melanosome in the investigated migmatite, which yielded an possible age of c. 2900 Ma, could have become incorporated in the basic protoliths of the migmatites by contamination during ascent of the original basic magma through continental crust.

The basement rocks of the Menderes Massif share many similarities with those of the Takab Complex. The older ages from this study are comparable to the detrital zircon age of 3140±2 Ma from the Menderes Massif [19]. The discovery of Archaean inheritance in the study area adds to the plate tectonic scenario of a regionally extensive Tethyan suture zone, extending from western Anatolia (Menderes Massif) through Eastern Anatolia (Bitlis Massif) to western Iran (Takab Complex - Zagros Zone) and the Central Iran Zone.

A further result of this study relates to the timing of partial melting in the migmatites of the Takab metamorphic core complex. Partial melting in the Takab area was probably the result of crustal thicking related to subduction and closure of the Neotethys ocean and consequent collision of the Arabian plate and the Iranian micro continents during the Tertiary Alpine Orogeny [2, 4, 15]. We have determined an age of 26.09±0.82 Ma for partial melting in the Takab Complex. This melting episode is considered to be the most likely source of the Tertiary granitoids associated with the Late Oligocene crustal thickening. This is in agreement with findings by [15]. On the basis of detrital zircon ages and the timing of initial synorogenic sedimentation, [15] place the Arabia–Eurasia collision in Iran between the middle Eocene and late Oligocene.

A widespread late extensional event leading to lithospheric thinning affected the rocks in the area after the Oligocene crustal thickening. K-Ar dating of graphitic schists in the Zarshuran area [26], apatite U-Th/He data from the Mahneshan area [41], and ^{40}Ar-^{39}Ar dating of muscovite schists [8] constrain the timing of significant exhumation of the rocks to post-date 20 Ma. Ages of c. 19 Ma ($^{40}Ar/^{39}Ar$ hornblende age; [14]) and c.16 Ma (K-Ar age; [6]) from granitoids in Turkey are considered to correspond to cooling and exhumation of the Menderes Massif [5], synchronous with cooling and exhumation of the Takab complex.

Also our findings show that at least some Iranian core complexes are Oligocene in age, not only Eocene as [44] argue.

Acknowledgements

This work is partly supported by University of Tabriz. We thank Prof. A.S. Sergei for his assistance with SHRIMP analysis and Prof. P. O'Brien and Prof. R. Bousquet for valuable helps and discussion. Constructive comments on an earlier version of the manuscript by R. Milke are highly appreciated. We are grateful to anonymous revierwrs of the journal and to Prof. Noori-Daloii for effiecient editorial handling of the manuscript.

References

1. Ahrens L. H. Implications of the Rhodesia age pattern. *Geochim. Cosmochim. Acta*. **8**: 1-15(1955).
2. Agard P., Omrani J., Jolivet L., Mouthereau F. Convergence history across Zagros (Iran): Constraints from collisional and earlier deformation. *Int. J. Earth Sci.*, **94**: 401–419 (2005).

3. Baldwin S.L., Ireland T.R. A tale of two eras: Pliocene-Pleistocene unroofing of Cenozoic and late Archean zircons from active metamorphic core complexes, Solomon Sea, Papua New Guinea. *Geology*, **23**: 1023-1026 (1995).
4. Berberian F., Muir, I.D., Pankhurst R.J., Berberian M. Late Cretaceous and early Miocene Andean-type plutonic activity in northern Makran and Central Iran. *J. Geol. Soc. Lond.n*, **139**: 605–614 (1982).
5. Bozkurt E., Oberhänsli R. Menderes Massif (Western Turkey): structural, metamorphic and magmatic evolution – a synthesis. *Int. J. Earth Sci.*, **89**: 679–708 (2001).
6. Delaloye M., Bingöl E. Granitoids from western and northwestern Anatolia: Geochemistry and modeling of geodynamic evolution. *Int. Geol. Rev.*, **42**: 241–268 (2000).
7. Fraser G., Ellis D., Eggins S. Zirconium abundance in granulite-facies minerals, with mplications for zircon geochronology in high-grade rocks. *Geology*, **25**: 607–610 (1997).
8. Gilg H.A., Boni M., Balassone G., Allen C.R., Banks D., Moore F. Marble-hosted sulfide ores in the Angouran Zn-(Pb–Ag) deposit, NW Iran: interaction of sedimentary brines with a metamorphic core complex. *Mineral. Depos.*, **41**: 1–16 (2006).
9. Golonka J. Plate tectonic evolution of the southern margin of Eurasia in the Mesozoic and Cenozoic. *Tectonophysics*, **381**: 235-273 (2004).
10. Hajialioghli R., Moazzen M., Droop G.T.R., Oberhansli R., Bousquet R., Jahangiri A., Ziemann M. Serpentine polymorphs and P-T evolution of meta-peridotites and serpentinites in the Takab area, NW Iran. *Min. Mag.*, **71**: 155–174 (2007a).
11. Hajialioghli R., Moazzen M., Jahangiri A., Droop G.T.R., Bousquet R., Oberhänsli R. Petrogenesis of meta-peridotites in the Takab area, NW Iran. *Goldschmidt Conference Abs., Cologne, Germany,* A370. (2007b).
12. Hajialioghli R., Moazzen M., Jahangiri A., Oberhänsli R., Mocek B., Altenberger U. Petrogenesis and tectonic evolution of metaluminous sub-alkaline granitoids from the Takab Complex, NW Iran. *Geol. Mag.*, **148**: 250-268 (2010).
13. Hassanzadeh J., Stockli D.F., Horton B.K., Axen G.J., Stockli L.D., Grove M., Schmitt A.K., Walker B.K. U-Pb zircon geochronology of late Neoproterozoic-Early Cambrian granitoids in Iran: Implications for paleogeography, magmatism and exhumation history of Iranian basement. *Tectonophysics*, **451**: 71-96 (2008).
14. Hetzel R., Passchier C.W., Ring U., Dora O.O. Bivergent extension in orogenic belts-the Menderes massif (southwestern Turkey). *Geology*, **23**: 455–458 (1995).
15. Horton B.K., Hassanzadeh J., Stockli D.F., Axen G.J., Gillis R.J., Guest B., Amini A., Fakhari M.D., Zamanzadeh S.M., Grove M. Detrital zircon provenance of Neoproterozoic to Cenozoic deposits in Iran: Implications for chronostratigraphy and collisional tectonics. *Tectonophysics*, **451**: 97-122 (2008).
16. Keay S., Lister G., Buick I. The timing of partial melting, Barrovian metamorphism and granite intrusion in the Naxos metamorphic core complex, Cyclades, Aegean Sea, Greece. *Tectonophysics*, **342**: 275–312 (2001).
17. Kelsey D., Clark C., Hand M. Thermobarometric modelling of zircon and monazite growth in melt-bearing systems: examples using model metapelitic and metapsammitic granulites. *J. Met. Geol.*, **26**: 199–212 (2008).
18. Kim N., Cheong C., Prak K., Kim J., Song Y., Crustal evolution of northeastern Yeongnam Massif, Korea, revealed by SHRIMP U–Pb zircon geochronology and geochemistry. *Gondwana Res.*, **21**: 865–875 (2012).
19. Kröner A., Şengör A.M.C. Archean and Proterozoic ancestry in late Precambrian to early Paleozoic. *Geology*, **18**: 1186-1190 (1990).
20. Liu X. C., Jahn B. M., Hu J., Li S. Z., Liu X., Song B.Metamorphic patterns and SHRIMP zircon ages of medium-to-high grade rocks from the Tongbai orogen, central China: implications for multiple accretion/collision processes prior to terminal continental collision. *J. Met. Geol.*, **29**: 979-1002 (2011).
21. Loos S., Reischmann T. The evolution of the southern Menderes Massif in SW Turkey as revealed by zircon dating. *J. Geol. Soc. Lond.*, **156**: 1021-1030 (1999).
22. Lotfi M. Geological map of Iran, 1:100,000 series sheet Takht-e-Soleyman. *Geological Survey of Iran*. (2001).
23. Ludwig K.R. Users' Manual for Isoplot/Ex Version 2, A Geochronological Toolkit for Microsoft Excel. *Berkeley Geochron. Center, Spec. Publ.*, **1**, 60. (1999).
24. Ludwig K.R. Decay constant errors in U-Pb concordia-intercept ages. *Chem. Geol.*, **166**: 315-18 (2000).
25. Mehnert K.R. Migmatites and the Origin of Granitic Rocks. Elsevier, Amsterdam. 393 p. (1968)
26. Mehrabi B., Yardley B.W.D., Cann J.R. Sediment-hosted disseminated gold mineralization at Zarshuran, NW Iran. *Mineral. Depos.a*, **34**: 673–696 (1999).
27. Moazzen M., Oberhänsli R., Hajialioghli R., Möller A., Bousquet R., Droop G.T.R., Jahangiri A. Peak and post-peak P-T conditions and fluid composition for scapolite-clinopyroxene-garnet calc-silicate rocks from the Takab area, NW Iran. *Eur. J. Mineral.*, **21**: 149 – 162 (2009).
28. Möller A., O'Brien P.J., Kennedy A., Kröner A. Polyphase zircon in ultrahigh- temperature granulites SW Norway: constraints for Pb diffusion in zircon. *J. Met. Geol.*, **20**: 727–740 (2002).
29. Möller A., O'Brien, P.J., Kennedy A., Kröner A. Linking growth episodes of zircon and metamorphic textures to chemistry: an example from the ultrahigh-temperature granulites of Rogaland (SW Norway). In: Vance D, Müller W, Villa IM (eds) Geochronology: Linking the Isotopic Record with Petrology and Textures. *Geol. Soc. Lond. Spec. Pub.*, **220**: 65-81 (2003a).
30. Möller A., Hensen B.J., Armstrong R.A., Mezger K., Ballèvre M. U–Pb zircon and monazite age constraints on granulite-facies metamorphism and deformation in the Strangways Metamorphic Complex (central Australia). *Contrib. Min. Pet.*, **145**: 406–423 (2003b).
31. Monteleone B.D., Baldwin S.L., Webb L.E., Fitzgerald P.G., Grove M., Schmitt A. Evidence for late Miocene to Pliocene HP metamorphism in eclogites from the D'Entrecasteaux Islands, SE Papua New Guinea. *J. Met. Geol.*, **25**: 245–265 (2007).
32. Nabavi M.H. An introduction to the geology of Iran. *Geol. Surv. Iran* (in Persian) (1976).

33. Nadimi A. Evolution of the Central Iranian basement. *Gondwana Res.*, **17**: 324-333 (2006).
34. Oberhänsli R., Rimmelé G., Candan O., Okay A. Relics of high - pressure metamorphism in the bitlis massif (VAN region, E Turkey). *Mitt Öst. Mineral. Gesell.*, **150** (2005).
35. Ping J., Kröner A., Zhou G. SHRIMP zircon U–Pb ages and REE partition for high-grade metamorphic rocks in the North Dabie complex: Insight into crustal evolution with respect to Triassic UHP metamorphism in east-central China. *Chem. Geol.*, **328**: 49-69 (2012).
36. Ramezani J.,Tucker R.D. The Saghand Region, Central Iran: U-Pb geochronology, petrogenesis and implications for Gondwana tectonics. *Am. J. Sci.*, **303**: 622-665 (2003).
37. Rubatto D., Hermann J., Berger A., Engi M. Protracted fluid-induced melting during Barrovian metamorphism in the Central Alps. *Contrib. Mineral. Petrol.*, **158**: 739-755 (2009).
38. Sláma J., Košler J., Pedersen R.B. Behaviour of zircon in high-grade metamorphic rocks-evidence from Hf isotopes, trace elements and textural studies. *Contrib. Mineral. Petrol.*, **154**: 335–356 (2007).
39. Samani B., Zhuyi G., Xuetao G., Chuan T. Geology of Precambrian in central Iran; On the context of stratigraphy, magmatism and metamorphism. *Geosci. Geol. Surv. Iran*, **3**: 40–63 (1994).
40. Şengör A.M.C., Yilmaz Y., Sungurlu O. Tectonics of the Mediterranean Cimmerides: nature and evolution of the western termination of Palaeo-Tethys. In: Dixon, J.E., Robertson, A.H.F. (Eds.), The Geological Evolution of the Eastern Mediterranean. *Geol. Soc. Lond. Spec. Publ.*, **17**: 77–112 (1984).
41. Stockli D.F., Hassanzadeh J., Stockli L.D., Axen G., Walker J.D., Dewane T.J. Structural and geochronological evidence for Oligo-Miocene intra-arc low-angle detachment faulting in the Takab- Zanjan area, NW Iran. *Abs., Prog. Geol. Soc. Am.*, **36**: 319 (2004).
42. Stöcklin J. Possible ancient continental margin in Iran. In: Burk C.A., Drake C.L., The geology of continental margins. New York: Springer-Verlag, 873-887 (1974).
43. Tera F., Wasserburg G.J. U–Th–Pb systematics in three Apollo 14 basalts and the problem of initial Pb in lunar rocks. *Earth Planet. Sci. Lett.*, **14**: 281–304 (1972).
44. Verdel C., Wernicke B.P., Ramezani J., Hassanzadeh J., Renne P.R., Spell T.L. Geology and thermochronology of Tertiary Cordilleran-style metamorphic core complexes in the Saghand region of central Iran. *Geol. Soc. Am. Bull.*, **119**: 961–977 (2007).
45. Wetherill_G.W. Discordant uranium–lead ages. Trans. *Am. Geophysic. Uni.*, **37**: 320–326 (1956).
46. Wiedenbeck M., Alle P., Corfu F., Griffin W.L., Meier M., Oberli F., von Quadt A., Roddnick J.C.,Spiegel W. Three natural zircon standards for U–Th–Pb, Lu–Hf, trace element and REE analyses. *Geostand. Newslett.*, **19**: 1–23 (1995).
47. Williams I.S. U-Th-Pb geochronology by ion microprobe. In: Mckibben, M.A., Shanks, W.C. and Ridley, W.I. (eds). Applications of Microanalytical Techniques to Understanding Mineralization Processes. *Rev. Economic Geol.*, **7**: 1-35 (1998).
48. Williams I.S., Buick I.S., Cartwright I. An extended episode of early Mesoproterozoic metamorphic fluid flow in the Reynolds Range, central Australia. *J. Met. Geol.*, **14**: 29–47 (1996).
49. Zack T., Moraes R., Kronz A. Temperature dependence of Zr in rutile: empirical calibration of a rutile thermometer. *Contrib. Mineral. Petrol.*, **148**: 471–488 (2004).
50. Zhao G., Cao L., Wilde S.A., Sun M., Choe W.J., Li S. Implications based on the first SHRIMP U–Pb zircon dating on Precambrian granitoid rocks in North Korea. *Earth Planet. Sci. Lett.*, **251**: 365–379 (2006).
51. Zheng Y-F., Zhang S-B., Zhao Z-F., Wu Y-B., Li X., Li Z., Wu F-Y. Contrasting zircon Hf and O isotopes in the two episodes of Neoproterozoic granitoids in South China: implications for growth and reworking of continental crust. *Lithos*, **96**: 127–150 (2007).